CREEP OF HIGH SPEED STEELS
PART I – EXPERIMENTAL INVESTIGATIONS

H. Berns, C. Broeckmann and H. F. Hinz
Institut für Werkstoffe, Lehrstuhl Werkstofftechnik, Ruhr–Universität Bochum,
D-44780 Bochum,
Germany

Abstract High speed steel HS 6-5-3 quenched and tempered to 52 HRC was tested up to about 300h under constant tensile stress at 600°C and 650°C and compared to a matrix steel and to hot work steels investigated earlier. The long carbide particles within the eutectic net of the as-cast state reduce the minimum creep rate, while the larger interface areas between particles and matrix of the forged and PM states enhance local stress relaxation by diffusion, thus increasing the minimum creep rate. The creep behaviour of the HSS matrix comes close to that of hot work tool steel. The evolution of damage is, however, accelerated by fracture and decohesion of carbide particles, which reduces the life to rupture, increasingly so in the order of PM, forged, and as-cast states. The addition of cobalt or further particles to the PM state have a strengthening effect only at low stress.

Keywords: creep, damage, high speed steel, hot work steel, hot forming

INTRODUCTION

High speed steels (HSS), originally developed for cutting tools, have been successfully used for cold forming tools because of their relatively high toughness. Due to their excellent hot hardness they are also prone to serve in hot forming tools. In fact their microstructure consists of a tempered martensitic matrix similar to hot work tool steels (HWS) and of eutectic or even primary carbides. These hard carbide particles impede adhesion in metal-to-metal contact and abrasion by scale or mineral grains. Therefore HSS have performed well in tools for hot compaction of granular mineral

substances or sinter iron [1]. Tools for semi-hot forging of steels are a possible application of HSS because high stresses and intensive wear are involved. Hot extrusion of metal matrix composites (MMC) calls for tools of enhanced hot hardness and wear resistance as well. These examples are marked by cyclic loading of the tools and by a duration of contact with the work piece from less than a second up to a minute. In summing up 10^3 to 10^5 cycles we arrive at an overall contact time between some minutes and some 10 hours. The surface temperature of the tool is expected to stay below 650°C. Previous work showed that creep plays an important part even during short cycles and hot strength has to be replaced by time-dependant creep strength to judge a hot work tool. This holds also true for creep/fatigue interaction [2, 3, 4].

About 30 years ago the importance of creep was recognised for the size stability of containers in hot extrusion of aluminium alloys especially in cable sheathing. This led to experimental investigations on creep resistance of HWS [5, 6, 7, 8, 9] and on the design of tools [5, 11, 12]. There is, however, no respective data on HSS available. They differ from HWS mainly by the coarse carbides precipitated form the melt. These hard particles are creep resistant and may strengthen the matrix/particle composite. But as the creep deformation is confined to the matrix a decohesion or fracture of particles is liable to cause damage in the microstructure and reduce the creep life. It is the aim of this study to reveal creep and damage in HSS experimentally. As these are bound to depend on morphology and amount of carbide particles, different microstructures will be investigated in the time and temperature range of the above tooling examples. The results of the present part I form the basis of a finite element simulation of the creep behaviour in part II. This method is employed to follow up the creep/damage evolution and gain additional information which is not accessible by experiment.

EXPERIMENTAL

The investigation centres on the HSS grade HS 6-5-3 respectively M3 class 2. In the as-cast state (C) of an 80kg sand casting the M_2C/M_6C eutectic forms a net around the metal dendrites which include some primary MC particles (Fig. 1a). By annealing or by hot working of an ingot the M_2C was decomposed to MC/M_6C (Fig. 1b) and after a cross-sectional reduction ratio of >10 the net was stretched to a banded carbide structure which characterises the as-forged state F (Fig. 1c). In powder metallurgical production

the eutectic net of atomised powder is extremely fine and coagulates during compaction by hot isostatic pressing (HIP) to give a dispersion of fine globular particles in the PM state (Fig. 1d). To increase the amount of dispersed particles a high vanadium PM grade was included which is also high in carbon (PMCV). A PM cobalt grade was taken into account to modify the HSS matrix (PMCo). All three PM grades were hot worked, which rarely changed their carbide morphology. The chemical composition of all HSS investigated is given in the upper part of Table 1.

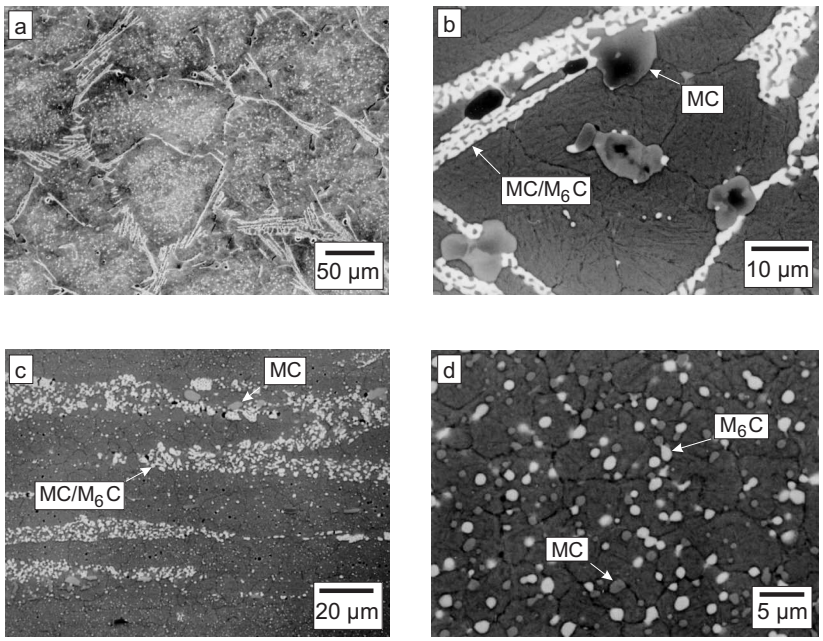

Figure 1. Microstructure of HSS, (a, b) as-cast, C, (c) forged, F, (d) PM.

In the lower part of this table we find a "matrix steel" (M), which resembles the matrix com-position of HS 6-5-3. It was found by thermodynamic calculations using ThermoCalc [10] for equilibrium at 1100℃ and compares well with experimental results of an HS 6-5-2 matrix. However, due to segregation some eutectic carbides appear locally, but their volume content stays below 1%. The hot work tool steels H11 and H13 are free of eutectic car-

Table 1. Chemical composition of the steel grades investigated (wt%)

grade	C	Cr	W	Mo	V	Si	Mn	Co
C	1.19	4.4	6.9	4.6	2.9	0.72	0.29	0.56
F	1.21	4.0	6.1	4.8	2.8	0.44	0.25	0.34
PM	1.31	3.9	5.9	4.9	2.9	0.60	0.27	0.50
PMCV	2.45	4.2	4.2	3.1	8.0	–	–	–
PMCo	1.31	4.2	6.0	5.1	3.0	0.66	0.28	8.9
H11	0.39	5.3	–	1.1	0.4	1.05	–	–
H13	0.4	5.0	–	1.4	1	1.1	0.4	–
M	0.48	4.3	1.9	2.0	0.6	0.54	0.35	–

bides except for some accidental particles in H13. Their creep behaviour was investigated earlier and they are included for comparison.

The as-cast specimes were taken from the core of the solidified cross-section, where equiaxed eutectic cells respectively globular primary grains prevail. The others were taken in longitudinal direction, i.e. in direction of hot working. All specimens were investigated in the hardened and tempered condition which is called initial state. Hardening was carried out in a vacuum furnace at 1180℃ (C, F, PM, PMCV), respectively 1140℃ (PMCo, M) for 10 minutes followed by quenching in a nitrogen stream of 5 bar pressure. After tempering twice at 650℃ for 2 hours the HSS specimens reached an average hardness of 52 HRC. The matrix steel M was tempered twice at 625℃ to reach a micro hot hardness close to the matrix of F, at least in the creep test range of 600 to 650℃. In previous work on creep of H11 and H13 the heat treatment conditions followed standard rules to reach a hardness of 44 to 47 HRC.

Light, scanning electron and transmission electron microscopy (LIM, SEM, TEM) were used to evaluate the microstructure before and after creep testing. The change of hot hardness HV 0.05 was measured in a vacuum chamber by heating the specimen and indenter [15]. Creep damage leads to pores which entail a change of density ρ. This was registered by the levitation method after elongation ε in slow tensile tests at 650℃ and a rate of $\dot{\varepsilon} = 5 \times 10^{-5} s^{-1}$. Flat creep specimens with edges to mount an extensometer (Fig. 2a) were held in a furnace under constant temperature and tensile stress

until necking. This was brought about by a lever arm under constant weight which gradually shortened to balance the reduction of cross section caused by creep elongation (Fig. 2b).

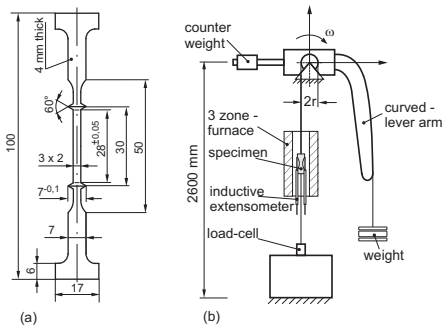

Figure 2. Creep testing, (a) specimen, (b) test rig.

This method of constant stress creep testing was proposed earlier by [16, 17] and achieved an accuracy within $\pm$ 3 MPa. Each of the three furnace zones was PID controlled by thermocouples to keep the temperature within $\pm$ 1℃. All creep data was derived computer assisted. Of the 111 creep tests, 99 were run until fracture. In addition a number of specimens were exposed to different degrees of creep deformation for metallographic inspection. The testing temperature was varied from 600℃ to 650℃ and the stress between 95 and 675 MPa to give fracture times t_f between about 5 and 300h, of which 70% remained below 60h.

RESULTS

MICROSTRUCTURE

The martensitic matrix contains carbides precipitated at different temperature levels: Primary and eutectic ones grow from the melt and their size decreases as the solidification rate increases. In the present cast HSS they extend to more than 10 µm in height (C, F, Table 2), while in the PM material they are spherodised by HIP to about 1 µm. Secondary carbides appear in the austenite during cooling from solidus temperature and obtain a globular shape of <1 µm by hot working and soft annealing. Of these the smaller

ones are dissolved at hardening temperature and again precipitated during tempering to a size of <0.1 µm. As the secondary and temper carbides hardly differ from grade to grade, they are attributed to the matrix. Thus this term comprises the steel lattice and "fine" carbide precipitates as opposed to the "coarse" ones solidified from the melt, which are designated as "particles". In PM grades these are hardly larger than the secondary carbides and equal in shape. The resulting uncertainty of telling them apart is negligible, though. The main difference between the C, F and PM grades investigated is caused by the morphology of particles and characteristic parameters are given in Table 2. Examples of the matrix microstructure are depicted in Fig. 3a.

Table 2. Mean parameters of initial microstructure: volume content f, diameter d, spacing s, height/width h/w

grade	f_P [%]	d_P [µm]	h/w	s_P [µm]	s_n [µm]	s_b [µm]	d_g [µm]
M	–	–	–	–	–	–	16.0
C	11.2	2.9 (1)	23.9 ± 14.0	1.44 (2)	83.5	–	83.5
F	9.2	3.96 (3)	7.7 ± 3.8	7.64 (4)	–	27.0	13.0
PM	11.4	1.0 ± 0.5	1.0	1.6	–	–	9.0
PMCV	18.3	1.2 ± 0.4	1.0	1.3	–	–	11.2
PMCo	11.5	1.2 ± 0.5	1.0	1.9	–	–	6.0

indices: carbide particle P, eutectic net n, carbide band b, austenitic grain g, (1) width, (2) within eutectic (3) taken as spheres of equal volume, (4) even dispersion assumed instead of bands

The hot hardness of the initial state drops continuously up to 650℃ and is considerably lower for M as compared to C in the range of 300 to 500℃ (Fig. 4). The tempering temperature of 650℃ was chosen to coincide with the highest service temperature. Although it lies above the peak of secondary hardening, softening of the matrix will occur after prolonged holding in the creep test range even without stress (Fig. 4b). This is accompanied by the growth of temper carbides and the formation of subgrains (Fig. 3b).

After the creep stress σ is applied, dislocation strengthening, recovery and growth of carbides occur in the matrix (Fig. 3c-g). At some creep elongation damage becomes visible. In the matrix steel M we observe the common generation of pores at grain boundaries (Fig. 5a). In PM material a rather large elongation is required to provoke decohesion of the globular particles from the matrix (Fig. 5b). At high stress and a lower temperature the as-cast

state C fails at a fracture elongation $\varepsilon_f \approx 1\%$ without noticeable damage. Under a lower stress and higher temperature particles of high aspect ratio oriented in the direction of σ fracture several times and compact ones show decohesion in the direction of σ (Fig. 5c, d). Particle fracture and decohesion hold also true for the forged state F (Fig. 5e, f). Both give rise to pores and cracks which lower the density of the steel. This is more pronounced in F than in PM (Fig. 6) and speaks for a slower damage accumulation in the latter.

CREEP TESTING

To start with, the creep elongation ε is recorded over time t. From this the first derivative with respect to t or ε may be obtained of which the latter was chosen to evaluate the minimum creep rate $\dot{\varepsilon}_{\min}$. Examples are given in Fig. 7. They reveal an intense strengthening within the primary creep range and thus $\dot{\varepsilon}_{\min}$ is reached after an elongation $\varepsilon_{\dot{\varepsilon}_{\min}}$ of less than 1%. There is hardly a secondary creep range of constant creep rate $\dot{\varepsilon}$ visible, so that the tertiary range of softening prevails above $\varepsilon_{\dot{\varepsilon}_{\min}}$. If we choose to characterise the creep resistance, the HSS improve in the order of PM, F, C. From an engineering point of view creep life may be as important and in this respect the sequence is reversed. The matrix steel M performs well in either way.

The dependence of $\dot{\varepsilon}_{\min}$ on σ is shown in Fig. 8 and fulfils NORTON's law for a given temperature [18], with μ representing the shear modulus.

$$\dot{\varepsilon}_{\min} = \mathrm{B}\ (\sigma/\mu)^n \tag{1}$$

The exponent n is represented by the slope of a double-logarithmic plot. At 600℃ the stress sensitivity increases in the order of C,M, PM, F, while at 650℃ it is C, F , PM (Fig. 8). From Fig. 9a, b follows that Co increases n of powder steels and $\dot{\varepsilon}_{\min}$ at higher stress. The same holds true for an increase of the particle volume (Fig. 9c). At 600℃ matrix steel M comes close to HWS, while it appears to be more resistant at 650℃ (Fig. 10, [19]). Except for F there is hardly any stress sensitivity visible for ε_f at 600℃ with PMCo at the upper and C at the lower end of ductility (Fig. 11a).

The validity of the MONKMAN–GRANT relation [20]

$$\mathrm{t}_f = \mathrm{C}_{\mathrm{MG}} \times\ \dot{\varepsilon}_{\min}^{-\mathrm{m}_{\mathrm{MG}}} \tag{2}$$

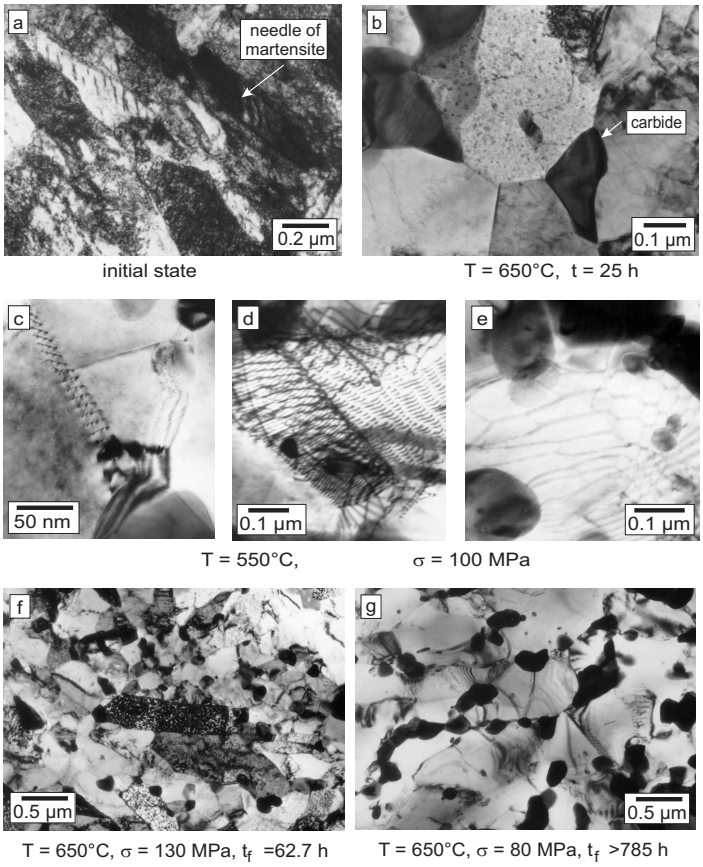

Figure 3. TEM micrographs of the matrix: (a) quenched and tempered 2 x 650℃, 2h (b) subgrains after additional tempering, (c) and the following after creep, dislocation pile-up in front of a carbide, (d) dislocation network, (e) subgrain, (f, g) growth of subgrains and carbides, (a, b, f, g) = grade C, (c, d, e) = grade F.

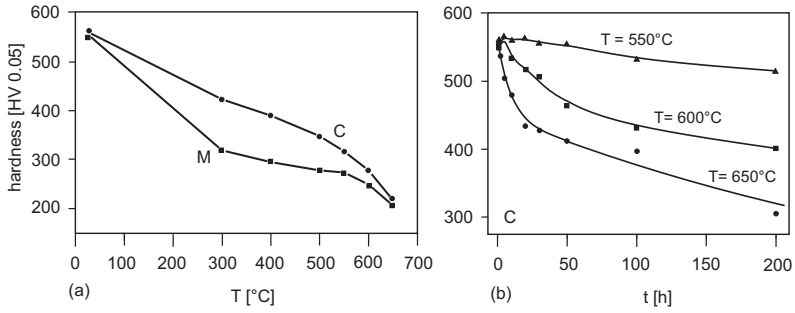

Figure 4. Hardness of the matrix, (a) hot hardness depending on the testing temperature T (b) tested at room temperature after tempering the initial state at T for a time t.

is controlled by a double-logarithmic plot of t_f over $\dot{\varepsilon}_{\min}$. The MONKMAN–GRANT exponent m_{MG} comes close to 1 for PM at 600°C and F at 650°C, while C at 600°C deviates most (Fig. 11b). A plot of σ over t_f yields "designs curves" for the matrix (M, H13) and for HSS with a slope of -1/ν (Fig. 12). If plotted over the LARSON–MILLER parameter [21]

$$P = T(C + \log t_f) \tag{3}$$

they more or less fall into one scatter band (Fig. 13). Finally an ARRHENIUS plot of log $\dot{\varepsilon}_{\min}$ over the reciprocal absolute temperature leads to the apparent activation energy Q_a (Fig. 14) and a sequence of C, M, F, PM already encountered in Fig. 7c.

DISCUSSION

CREEP OF MATRIX

The time-dependence of high-temperature strength became important in the wake of e.g. fossile power plants and petrochemistry. By 1935 it was incorporated into the design of components [22]. Until about 1970 long-time creep testing prevailed and quenched and tempered steels with 0.1 to 0.25 wt% C played an important part [23]. These creep resistant steels were tempered just below Ac1 to bring the temper carbides close to equilibrium. In contrast, the investigation of creep in quenched and tempered HWS, starting

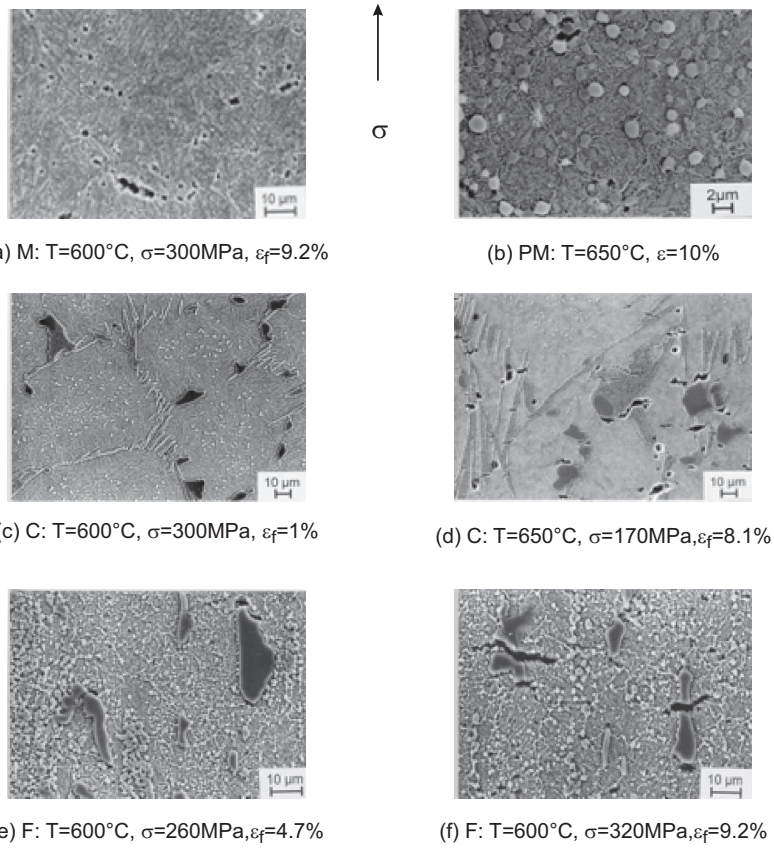

(a) M: T=600°C, σ=300MPa, ε_f=9.2%

(b) PM: T=650°C, ε=10%

(c) C: T=600°C, σ=300MPa, ε_f=1%

(d) C: T=650°C, σ=170MPa,ε_f=8.1%

(e) F: T=600°C, σ=260MPa,ε_f=4.7%

(f) F: T=600°C, σ=320MPa,ε_f=9.2%

Figure 5. Examples of creep damage outside of the necking area, (b) was taken from a hot tensile test specimen pulled at a rate of $\dot{\varepsilon} = 5 \times 10^{-5} s^{-1}$.

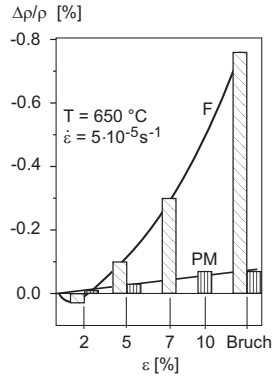

Figure 6. Change of density ρ depending on elongation ε in slow hot tensile tests.

around 1970 [12], dealt with a microstructure of lower phase stability but higher strength due to a lower tempering temperature and a greater volume of precipitates. This tendency is even more pronounced for HSS at peak hardness, the matrix of which contains only half of the potential carbide volume, while the remainder is precipitated during service [24, 25].

Recent work on hot and creep strength of HSS [26] showed, that it does not make sense to start with a peak harness of 65 HRC corresponding to a tempering temperature of 550°C because of immediate softening at service temperature up to 650°C. Therefore the HSS of the present study is over-aged by tempering at the highest expected service temperature resulting in a hardness of 52 HRC which comes closer to that of HWS. The as-tempered microstructures of HSS and HWS are similar as well [5, 26]. However, the amount of fine precipitates may reach 10 wt% in HSS [13, 14] compared to 5 wt% in HWS [6] and 2 wt% in creep resistant steel. In the latter all carbides are precipitated by tempering but change their composition and structure during service towards a more stable state closer to equilibrium, see e.g. [27]. This change happens in HWS [12] and HSS [25], too, but in addition carbides are precipitated after tempering, although not to same extent as in peak tempered steel. This additional precipitation occurs mainly during the primary creep stage and provokes an intense strengthening which comes along with a reduction of $\dot{\varepsilon}_{\min}$ by almost two orders of magnitude (Fig. 7c).

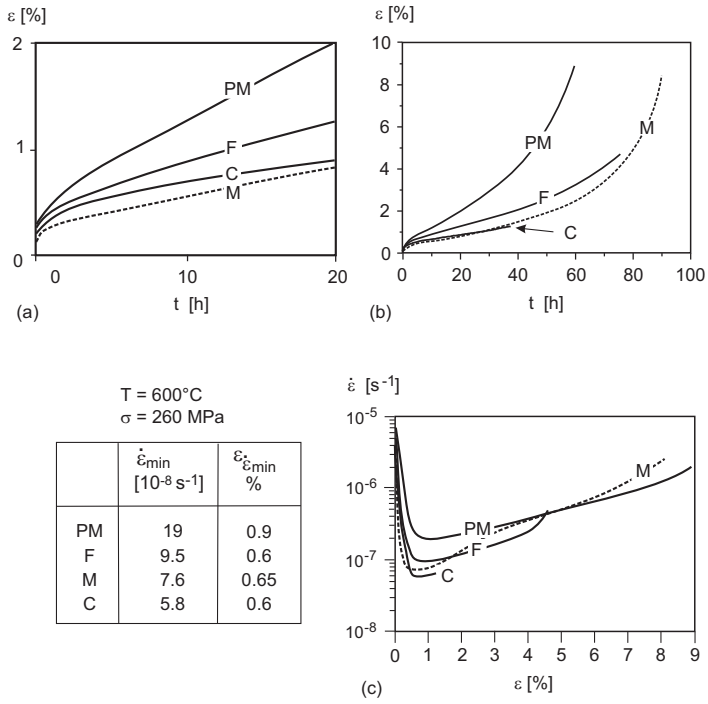

	$\dot{\varepsilon}_{min}$ [10^{-8} s^{-1}]	$\varepsilon_{\dot{\varepsilon}_{min}}$ %
PM	19	0.9
F	9.5	0.6
M	7.6	0.65
C	5.8	0.6

Figure 7. Examples of creep curves, (a) elongation ε recorded over time t, initial part, (b) as before, total curve, (c) first derivative with respect to ε from which the minimum creep rate $\dot{\varepsilon}_{\min}$ and the elongation $\varepsilon_{\dot{\varepsilon}_{\min}}$ to reach it are taken.

The primary creep stage of HWS follows ANDRADE's law

$$\varepsilon_{\mathrm{p}} = \beta \mathrm{t}^{\mathrm{m}} \tag{4}$$

A semi-logarithmic plot of plastic elongation ε_{p} over time t gave m = 0.33 for lead [28] but only m $\approx$ 0.1 for HWS at 550℃, increasing with stress [6]. This pointed to intensive strain hardening by dislocation pile-up in front of fine carbides and the stress dependence indicated a joint effect of additional carbides precipitated within the first percent of plastic elongation [12]. This holds true for HSS as well as demonstrated by $\dot{\varepsilon}_{\min}$ <1% in Fig. 7. The present tempering temperature of HSS is 30 to 50℃ above the common

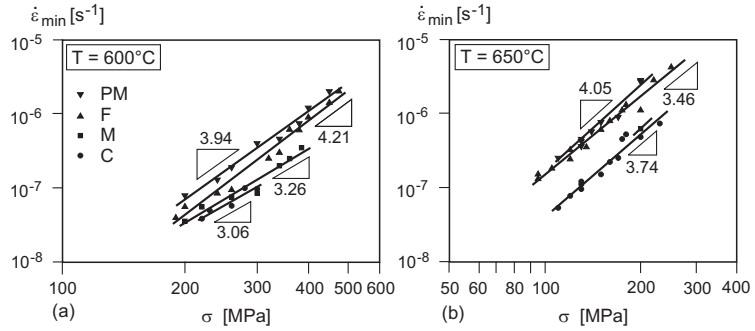

Figure 8. Minimum creep rate $\dot{\varepsilon}_{\min}$ depending on creep stress σ, influence of particle morphology and temperature, triangles indicating the slope.

treatment for e.g. H13 and both are tempered about 90℃ above their peak of secondary hardening. Therefore it seems reasonable to assume that their matrix potential, i.e. the share of carbide precipitation after tempering during service [24], is about equal in spite to the overall amount of precipitates in the matrix being twice as high for HSS.

Heating alone decreases the hardness of HSS (Fig. 4b), which is accelerated by superimposed creep. The ratio of hardness inside and outside the test length of creep specimens amounted to an average of 0.86 after creep rupture. A similar observation was made for HWS [12]. This softening is caused by carbide growth (Fig. 3f, g), which entails a growth of subgrains, that develop from dislocation networks (Fig. 3d, e). Starting from the high dislocation density of virgin HSS martensite, recovery occurs already during tempering (Fig. 3a, b) and subsequently during creep (Fig. 3c-e). The subgrain size is apparently restricted by the spacing of the surrounding temper carbides (Fig. 3f, g).

The softening processes, recovery and growth of carbides plus subgrains, act from the very beginning and stay active throughout service. This is also true for dislocation strengthening, but the other strengthening process of concurrent precipitation seems to expire after the first percent of plastic elongation. As a result of strengthening and softening $\dot{\varepsilon}_{\min}$ is reached at $\dot{\varepsilon}_{\min}$ (Fig. 7c). Because creep at this point is not solely depending on an

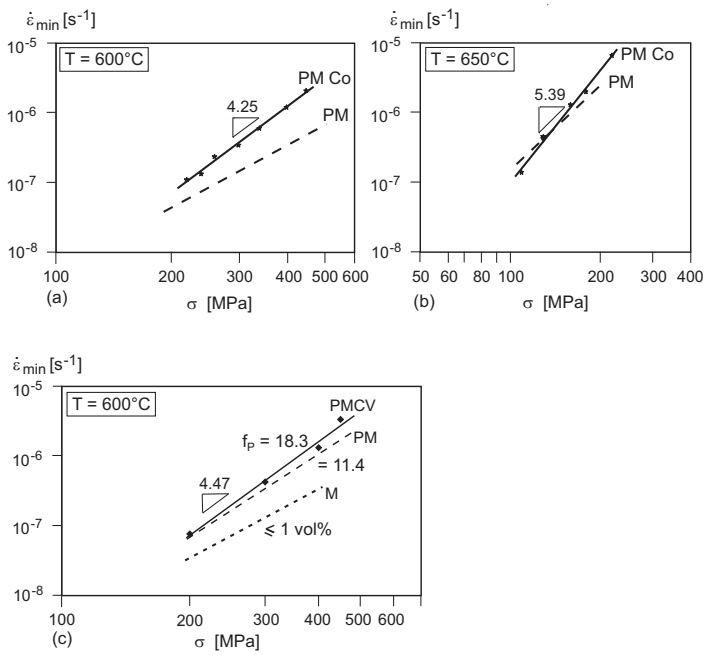

Figure 9. Minimum creep rate $\dot{\varepsilon}_{\min}$ depending on creep stress σ, (a, b) influence of Co, (c) influence of particle volume f_P, triangles indicating the slope.

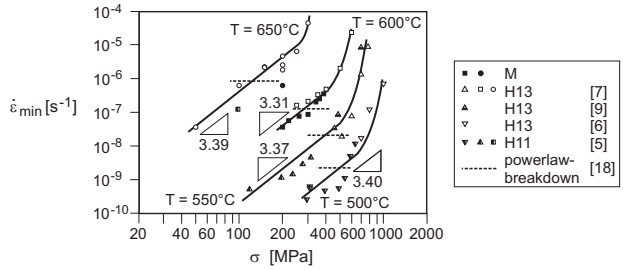

Figure 10. Minimum creep rate $\dot{\varepsilon}_{\min}$ of matrix steel M compared with that of hot work tool steels H11 and H13 taken from the literature, triangles indicate the slope.

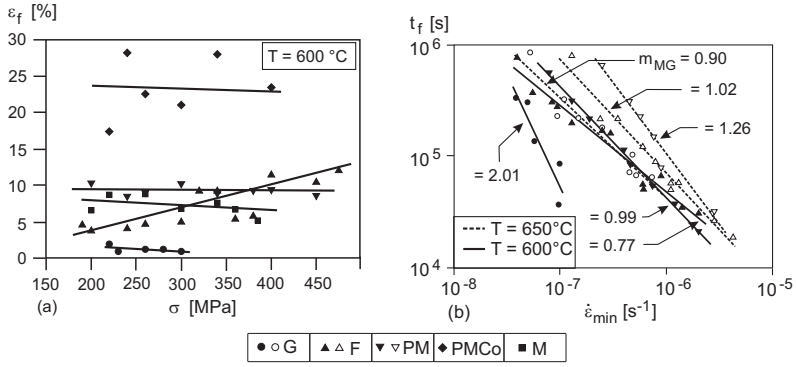

Figure 11. (a) elongation to fracture e_f depending on applied stress σ, (b) time to fracture t_f depending on the minimum creep rate $\dot{\varepsilon}_{\min}$, m_{MG} denotes the exponent of the MONKMAN–GRANT relation in equation (2).

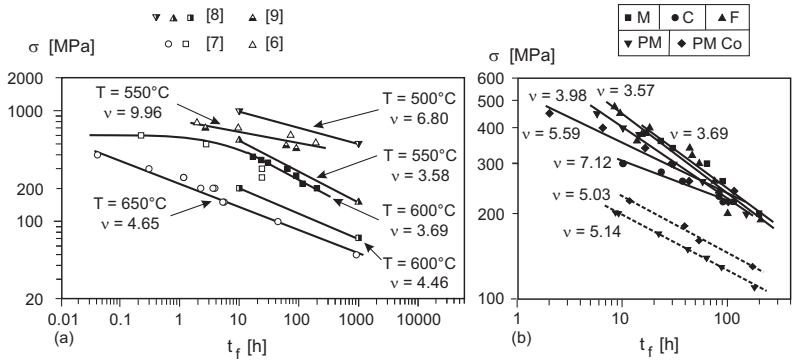

Figure 12. Influence of stress and testing temperature on fracture time t_f of (a) matrix steel M and hot work tool steel H13 taken from [6-9], (b) HSS and M (the slope is - $1/\nu$).

equilibrium of generation and annihilation of dislocations, a secondary creep stage of constant $\dot{\varepsilon}$ is not to be expected, although a plot of ε over time suggests a limited linearity (Fig. 7a, b). Damage is not yet observed at $\varepsilon_{\dot{\varepsilon}_{\min}}$ and therefore not a cause of softening at this stage.

The stress dependence of $\dot{\varepsilon}_{\min}$ allows to compare different steels at a given temperature. The matrix steel M and the HWS show a similar performance

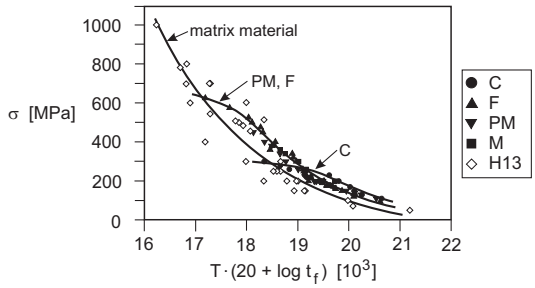

Figure 13. LARSON–MILLER representation of creep results obtained for different steels and testing temperatures, H13 taken from [6, 7, 8, 9].

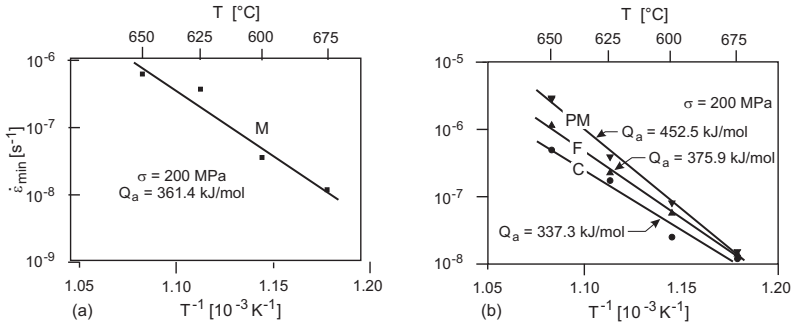

Figure 14. Plot to derive the apparent activation energy Q_a, (a) matrix steel M , (b) HSS grades.

(Fig. 10) and are even close to the HSS grades in Fig. 8. This supports the above conclusion that the microstructural changes in HSS and HWS up to $\dot{\varepsilon}_{\min}$ are similar. It also points out that the early stage of creep in HSS is governed by the matrix. The mean slopes of about 3.7 in Fig. 8 and in 3.4 in Fig. 10 indicate that there is no threshold stress σ_{th} involved [29, 30, 31, 32] and the NORTON exponent n of eq. 1 is not an apparent but a true one. At higher stress the exponent was found near 7 for PM, respectively 9 for F in strain rate controlled tests at 650℃ [26], revealing that σ_{th} sets in at higher creep rates. As the strengthening and softening processes leading to $\dot{\varepsilon}_{\min}$ depend on diffusion, the activation energy Q_a was derived by an ARRHENIUS plot of $\dot{\varepsilon}_{\min}$. The apparent values shown in Fig. 14 are transformed into the

true ones Q_c by taking the temperature dependence of the shear modules into account. The values are Q_c = 343 kJ/mol for M and Q_a = -24 kJ/mol for PM, F and C. They are far above the values of iron self diffusion and even considerably above the diffusion of alloying elements in iron. This leads to the conclusion that the diffusion of solute atoms and a resulting drag of dislocations is not the only process involved and that the fine precipitates are contributing, too. This is supported by the fact that the powerlaw breakdown after [19], marked in Fig. 10, stays below the observed limit above which an exponential relation between $\dot{\varepsilon}_{\min}$ and σ becomes valid [5, 7].

The element Co is confined to the matrix, where it increases the concentration of free electrons, which support ordering of solute atoms in the parent austenite, so that the precipitation of carbides and their growth is retarded [33]. This entails a high matrix potential of the initial state which most effectively suppresses creep, if the test duration is long, i.e. the stress is low. In Fig. 9a, b the higher NORTON exponent of PMCo compared to PM leads to an intersection of both graphs at $\sigma \approx 130$ MPa and to a higher creep resistance below this point.

EFFECT OF CARBIDE PARTICLES

Effect on strength. The load carrying capacity of hard particles increases with their height to width (h/w) aspect ratio. Based on the shear lag approach [34] and additional considerations in [35, 36, 37] it was demonstrated, that the round particles of PM grades do not strengthen the "composite" while the extended ones of grade C do [38]. Grade F was located inbetween. This sequence is supported experimentally by a plot of s over the time tp1 to reach ε_{p} = 1%, which is within the range of $\dot{\varepsilon}_{\min}$. The creep resistance increases in the order of PM, F, C (Fig. 15). Compared to M the creep rate of C is lower while those of F and PM are higher (Fig. 7 and 8). This points to an effect of phase boundary diffusion, by which the interfacial stresses are continuously relaxed. This is the more pronounced, the larger the overall carbide surface, which is - at a given carbide volume - highest for the smallest particle size encountered in PM. By comparing HSS with roughly 10 vol% of carbide particles to the matrix steel M with less than 1 vol% we realise, that the aspect ratio dominates the creep resistance of C, while rapid phase boundary diffusion prevails in F and PM.

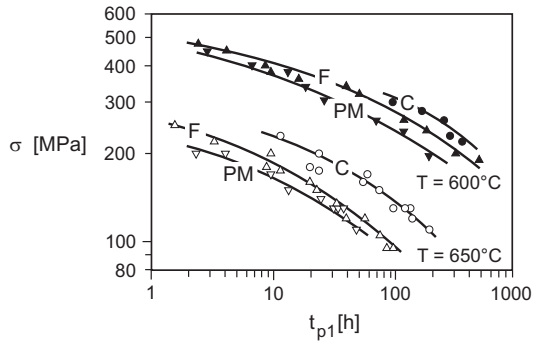

Figure 15. Stress σ to reach time t_{p1} at which plastic strain $\dot{\varepsilon}_{\mathrm{p}} = 1\%$.

Effect on damage. The right-hand curvature of the graph concerning M above $\dot{\varepsilon}_{\mathrm{min}}$ in Fig. 7c hints to softening by growth of precipitates [39], while the subsequent left-hand turn above about 4% of elongation is most likely associated with damage by pores along grain boundaries (compare Fig. 5a). The HSS reveal an overall left-hand curvature increasing towards fracture which points to an earlier damage by fracture and decohesion of particles (compare Fig. 5b-f). In addition the higher triaxiality of stress between particles [40] adds to the formation of pores in the matrix. However, the very first appearance of creep damage is hard to detect and depends on the magnification applied. It may well start soon above $\dot{\varepsilon}_{\mathrm{min}}$. The higher the load carrying capacity, i.e. the aspect ratio, the more liable the particles are to crack. The larger the particles the sooner they tend to fail, because they are more likely to contain defects [41, 42]. Therefore we don't see cracked particles in PM. In C and F the large and slender ones rupture first (Fig. 5). Decohesion starts at large particles and is therefore delayed in PM. As creep goes on the cracks and decohesions are widened to pores, which are much smaller in PM compared to F and lower the density accordingly (Fig. 6). Slight changes of density by phase transformations are superimposed, though, as indicated by the initial increase up to $\varepsilon = 2\%$.

As to the effect of particle distribution we observe an acceleration of damage to fracture in the sequence of C, F, PM. In the particle net of C the stress is concentrated in the eutectic, which together with a high aspect ratio

of the particles provokes early cracks. They extend along the net and cause fracture at a low value of ε_f (Fig. 11a). In the particle bands of F decohesion and fracture of particles require pore formation within the matrix to bridge the gap inbetween. That takes time, which is available at a lower stress causing a reduction of ε_f (Fig. 11a). The dispersion of particles in PM does not suffer from particle cracking and decohesion starts relatively late, because of ready stress relaxation around the comparatively small particles. Therefore ε_f of PM is even above M and only surpassed by PMCo. While M_3C is observed on former austenite grain boundaries of PM after creep (see also [43]), no embrittling precipitates are encountered in PMCo. Like Ni, Co tends to segregate into grain boundaries and the subsequent raise of carbon activity drives C out of this area, which explains the superior values of ε_f in PMCo (Fig. 11a). The addition of dispersed round particles lowers the creep resistance in the stress range tested (Fig. 9c), because the faster grain boundary diffusion is enhanced and stress relaxation around the particles along with it. At a lower stress the effect may be reversed, as softening via growth of precipitates and subgrains is not compensated by particles.

The Co-alloy Stellite 6 with nominally (wt%) 29 Cr, 5 W and 1.2 C was investigated in the as-cast, forged and PM condition for comparison. Already in tensile and impact tests the decisive effect of particle size and distribution became apparent [44]. Creep tests [45] revealed a damage evolution similar to HSS. A detailed comparison of M, C, F, PM to the respective Co-grades is given in [38].

Effect on life. The high MONKMAN–GRANT exponent of C in Fig. 11b already indicates that the most creep resistant grade does not live long enough to achieve prolonged service. This is reflected by the lowest ε_f in Fig. 11a. A general look at HSS creep curves shows a predominance of stage three in terms of total life time or elongation (Fig. 7). Damage evolution and life time are apparently closely related and therefore KACHANOV and RABOTNOV [46] introduced a damage variable ω into eq. 1, which extends from undamaged (ω = 0) to fracture (ω = 1).

$$\dot{\varepsilon} = \mathrm{B}\ (\sigma/\mu)^{\mathrm{n}}\ (1/(1-\omega)^{\mathrm{m}}) \tag{5}$$

$$\dot{\omega} = \dot{\omega}_0\ (\sigma/\mu)^{\nu})\ (1/(1-\omega)^{\eta}) \tag{6}$$

$\dot{\omega}$ is the rate of damage evolution and the initial value $\dot{\omega}_0$ may be used to derive the time to fracture t_f [38]

$$t_f = (\mu/\sigma)^{\nu} \; (\dot{\omega}_0(1+\nu)) \tag{7}$$

Plotting σ over t_f, as done in design curves, gives the exponent n (Fig. 12). For some grades n = ν is about fulfilled, which validates the MONKMAN–GRANT relation (eq. 2). If we try to as-sign a physical meaning to the mathematical variable ω, a model on the growth of pores up to intercrystalline fracture fits best [47]. At 600°C most HSS, HWS and M merge into $\sigma_{200h} \approx 200$ MPa. But at higher stresses, encountered in tooling operations, differences become apparent and e.g. σ_{10h} varies from 200 to 500 MPa with F and PM at the top. In terms of life we need a low $\dot{\varepsilon}_{\min}$ to start from and a slow growth of damage ω, expressed by a large ε_f, to achieve a good performance. This is underlined by the longer life of PMCo at 650°C compared to PM (Fig. 12b). Although both are rather close in respect to $\dot{\varepsilon}_{\min}$ (Fig. 9b), damage of PMCo is stretched over longer period of time as shown by the much higher ε_f in Fig. 11a. The same tendency is reflected by the LARSON–MILLER plot in Fig. 13, which combines test results derived at different temperatures. At the high end of T and / or t_f the HSS perform better than the matrix materials M and H13.

SUITABILITY IN SERVICE

At first sight the advantages of HSS over HWS appear to be marginal: The minimum creep rate of the overaged state is not improved, except for the brittle grade C, and life to fracture is hardly raised. One should, however, keep in mind that tensile tests enhance damage and the more so in HSS because of particles. In compressive tests the formation of pores, requiring a positive hydrostatic stress, is subdued and HSS are bound to profit most. During upset forging compressive stresses prevail and also in punches of extrusion tools. In the die of the latter we encounter a tensile hoop stress, though, but it may be reduced by a shrink fit. Therefore it seems reasonable to look at punches in hot forming first, which also suffer from wear at the edges. In this respect particles are expected to improve the performance, because they with-stand adhesion and abrasion. General rules reveal an influence of particle size and an advantage of dispersed particles [48]. This also applies to tools for hot compaction of granular substances. The user may be quite

satisfied with a creep resistance close to HWS, but highly appreciates the improvement of wear resistance by particles.

The directionality of properties in a banded microstructure was investigated for various steels and HWS among them [49]. Considering e.g. a container of an extrusion press, the highest stress, i.e. the hoop stress, acts transverse to the bands. The same holds true for thermal cycling, which is accompanied by tensile and compressive half cycles in the surface acting in longitudinal and transverse direction. It seems reasonable to assume that, because of the preferred particle orientation, creep damage of F is accumulated more rapidly under transverse loading, while hardly any directional change is to be anticipated for C and PM. In respect to the conditions encountered in service, creep tests with longitudinal tensile specimens may not resemble the worst case of loading for F, but appear too severe in relation to tools operated under compression. Still the present experimental investigation proves, that the creep behaviour of HSS is fair enough to take a closer look at the wear resistance, which is best recorded in field tests preferentially with simple cylindrical punches. It appears wise to start with PMCo of superior ductility and try F next. Recent work on thermal cyling by a laser spot up to 700℃ showed [50] that more heat checks are generated per unit surface area of PMCV compared to a hardened MMC containing carbide particles of the same volume content, but larger by almost two orders of magnitude in size. However, crack penetration perpendicular to the surface was much deeper for MMC. The dispersion of fine particles in powder steel refines the crack net thus dissipating the energy of crack extension and retarding damage by thermal fatigue. As to manufacturing, machining is feasible at 52 HRC and hardening is done in a vacuum furnace as applies to most HWS tools. HSS require a higher austenitising temperature, though. It is essential to preheat the tool, prior to service.

CONCLUSIONS

The investigation of creep in overaged as-cast (C), forged (F) and PM high speed steel HS 6-5-3 under constant tensile stress at temperatures of 600℃ and 650℃ led to the following conclusion:

(a) The matrix of high speed steel (HSS) reveals a creep behaviour, which comes close to that of hot work tool steel (HWS). After a combined dislocation and precipitation strengthening in the primary creep stage

up to about 1% plastic elongation, softening occurs by growth of precipitates and subgrains and> is later supported by damage and leads to an extended tertiary creep range.

(b) The elongated carbide particles within the eutectic net of C have a strengthening effect, while the smaller spheres of PM provoke softening, because of enhanced phase boundary diffusion.

(c) Compared to HWS the evolution of damage is faster in C and F because of particle fracture an decohesion in the carbide net, respectively carbide bands. Due to the dispersion of fine particles, damage of PM is delayed.

(d) Elongation at fracture is increased in the order of C, F, PM and even further in a PM grade containing about 9 wt% Co.

(e) In terms of creep resistance under tensile loading there hardly seems to be an advantage of HSS over HWS except for a higher wear resistance. However, tools like punches serve under compressive stresses, which suppress damage. This might be a field of application for HSS in which resistance to creep and to wear are required.

REFERENCES

[1] H. BERNS, C. BROECKMANN, W. THEISEN and B. WEWERS, Mat.wiss. u. Werkstofftechnik 32(5) (2001) 422.

[2] R. DANZER and F. STURM, Archiv für das Eisenhüttenwesen 53 (1982) 245.

[3] R. DANZER, Z. metallk. 78(1) (1987) 19.

[4] W. MITTER, K. HABERFELLNER, R. DANZER and C. STICKLER, HTM 52(4) (1997) 253.

[5] H. BERNS, Z. wirtschaftl. Fertigung 71(2) (1976)64.

[6] H. BERNS and F. PSCHENIZKA, Zeitschrift für Werkstofftechnik 11 (1980) 258.

[7] B. BUCHMAYR, R. DANZER, W. MITTER and B. H. PARK, Archiv für das Eisenhüttenwesen 53 (1982) 35.

[8] E. HABERLING, Thyssen Edelstahl Technische Berichte 13(2) (1987) 118.

[9] H. BERNS and F. WENDL, Radex-Rundschau 2 (1987) 375.

[10] B. SUNDMAN, Thermo-Calc User's Guide, Royal Institute of Technology, Stockholm (1997)

[11] H. WAWRA, Berechnung von Schrumpfverbindungen mit elastischer und nichtelastischer Formänderung unter zeitlich veränderlicher thermischer und mechanischer Belastung, doctoral thesis, TU München, FB Maschinenbau, München (1975)

[12] H. BERNS Z. metallk. 67(5) (1976) 283.

[13] E. HABERLING and I. SCHRUFF, Thyssen Edelstahl Technische Berichte 11(2) (1985) 99.

[14] K. BUNGARDT, E. HABERLING, A. ROSE and H. H. WEIGAND, DEW Technische Berichte 12(3) (1972) 111.

[15] M. LÜHRIG, " Termperaturabhängigkeit der Mikrohärte von Mischkristallen in Phasengemischen", Dissertation Ruhr-Universität Bochum, Fortschr.-Ber. VDI, Reihe 5, Nummer 297 (Düsseldorf, 1993)

[16] E.N.Da C. ANDRADE and B. CHALMERS, Proceedings - Royal Society of London A138 (1932) 348.

[17] W. BLUM and F. PSCHENITZKA, Z. Metallk., 67(1) (1976)62.

[18] F.H. NORTON, The Creep of Steel at High Temperatures (McGraw-Hill, 1929)

[19] P. YAVARI and T.G. LANGDON, Acta Metallurgica 30 (1982) 2181.

[20] F.C. MONKMAN and N.J. GRANT, in Proceedings of the ASTM annual meeting (Philadelphia, USA, Vol. 56, 1956) p.593

[21] F.R. LARSON and J. MILLER, Transactions of the American Society of Mechanical Engineering (1952) 765.

[22] R.W. BAILEY, Utilisation of creep test data in engineering design, Proc. Inst. Mech. Eng., 131–349, 131 (1935)

[23] H. FABRITIUS et al. Steel, Springer Verlag Berlin 2: applications (1993) 226.

[24] S. KARAGÖZ, H. F. FISCHMEISTER and H.-O. ANDRÈN, Metallurgical Transactions A 23A (1992) 1631.

[25] H. F. FISCHMEISTER, S. KARAGÖZ and H.-O. ANDRÈN, Acta Metallurgica 36 (1988) 817.

[26] H.-F. HINZ, "Einfluß der Karbidmorphologie auf die Warmfestigkeit von Schnellarbeitsstahl", Dissertation, Ruhr-Universität Bochum, Fortschr.-Ber. VDI, Reihe 5, Nummer 564, (Düsseldorf, 1999)

[27] D. HORSTMANN et al., Vorgänge im Mikrogefäge von Cr-Mo-V-Stählen während einer Zeitstandbeanspruchung, Arch. Eisenhüttenwesen, 711–717, 45(10) (1974)

[28] E.N.Da C. ANDRADE, Proceedings - Royal Society of London A84 (1911) 1.

[29] L. M. BROWN in Fatigue and Creep of Compistie Materials - Proc. of the 3rd Risø International Symposium on Metallurgy and Materials Science, edited by H. Lilholt and R. Talreja (Risø National Laboratory, Roskilde, D'änemark, 1982) Mechanics and Physics of Solids 14 (1966) 177.

[30] M. McLEAN, Acta Metallurgica 33(4) (1985) 545.

[31] E. ARZT and P. GRAHLE, Z. Metallk. 87(11) (1996) 874.

[32] J. LIN and O. D. SHERBY, Res. Mechanica 2 (1981) 251.

[33] Cobalt Monograph (Centre d'Information du Cobalt, Belgien, 1960)

[34] A. KELLY and W. R. TYSON, Journal of Mechanics and Physics of Solids 14 (1966) 177.

[35] S. T. MILEIKO, Journal of Materials Science 5 (1970) 254.

[36] V.C. NARDONE and K. M. PREWO, Scripta Metallurgica 20 (1986) 43.

[37] J. RÖSLER, G. BAO and A.G. EVANS, Acta Metallurgica et Materialia 39(11) (1991) 2733.

[38] C. BROECKMANN, "Kriechen partikelverstärkter metallischer Werkstoffe" (Habilitationsschrift Ruhr-Universit'ät Bochum, Fortschr. Ber. VDI, Reihe 5, Nummer 612, 2001)

[39] W. BLUM and B. REPPICH, in "Creep Behaviour of Crystalline Solids" edited by B. Wilshire and R. W. Evans (Verlag: Pineridge Press, Swansea, UK, 1985) p.83

[40] T. CHRISTMAN, A. NEEDLEMAN and S. SURESH, Acta Metallurgica 37(11) (1989) 3029.

[41] Y. BRECHET, J. D. EMBURY, S.TAO and L. LUO, Acta Metallurgica et Materialia 39 (1991) 1781.

[42] P. M. SINGH and J. J. LEWANDOWSKI, Metallurgical Transactions A 24A(11) (1993) 2531.

[43] R. WANG, H.-O. ANDRÉN, H. WISELL and G. L. DUNLOP, Acta Metallurgica et Materialia 40(7) (1992) 1727.

[44] H. BERNS and F. WENDL, in Proceedings of the 2nd International Conference on Cobalt (Venedig, Italien, 1985)

[45] O. LÜSEBRINK, "Einfluß grober Partikel auf die Kriechrißausbreitung am Beispiel einer Kobalthartlegierung" (Dissertation, Ruhr-Universität Bochum, Fortschr. Ber. VDI, Reihe 5, Nummer 604, Düsseldorf, 200)

[46] F. A. LECKIE and D. R. HAYHURST, Acta Metallurgica 25 (1977) 1059.

[47] A. C. F. COCKS and M. F. ASHBY, Progress in Materials Science 27 (1982) 189.

[48] H. BERNS in “Hartlegierungen und Hartverbundwerkstoffe”, chapter Einleitung, edited by H. Berns (Springer, Berlin Heidelberg New York, 1998) p.5.

[49] H. BERNS in "Tool Materials for Molds and Dies" edited by G. Krauss and H. Nordberg (The Colorade School of Mines Press, Denver, USA, 1987)

[50] B. WEWERS "Verschleißbest'ändige MM mit in situ TiC-Partikeln" (doctoral thesis, Ruhr-Universität Bochum, Bochum, 2002)